Computers and Concrete, Vol. 4, No. 2 (2007) 119-134
DOI: http://dx.doi.org/10.12989/cac.2007.4.2.119

Nonlinear analysis of RC beams strengthened by externally bonded plates

Jae-Guen Park†, Kwang-Myong Lee‡ and Hyun-Mock Shin‡†

Department of Civil and Environmental Engineering, Sungkyunkwan University, 300 Chunchun-dong, Jangan-gu, Suwon, Kyonggi-do, 440-746, Korea

Yoon-Je Park‡‡

Structural Division, S & Q Engineering Co, Ltd, Seoul, Korea

(Received September 21 2006, Accepted March 23, 2007)

Abstract. External bonding of steel or FRP plates to reinforced concrete (RC) structures has been a popular method for strengthening RC structures; however, unexpected premature failure often occurs due to debonding between the concrete and the epoxy. We proposed a Coulomb criterion with a constant failure surface as the debonding failure criterion for the concrete-epoxy interface. Diagonal shear bonding tests were conducted to determine the debonding properties that were related to the failure criterion, such as the angle of internal friction and the coefficient of cohesion. In addition, an interface element that utilized the Coulomb criterion was implemented in a nonlinear finite element analysis program to simulate debonding failure behavior. Experimental studies and numerical analysies on RC beams strengthened by an externally bonded steel or FRP plate were used to determine the range of the coefficient of cohesion. The results that were presented prove that premature failure loads of strengthened RC beams can be predicted with using the bonding properties and the finite element program with including the proposed Coulomb criterion.

Keywords: Coulomb criterion; debonding; interface element; nonlinear finite element analysis premature failure; strengthening.

1. Introduction

The bonding of steel or FRP plates with using epoxy resins has been widely used to strengthen reinforced concrete (RC) structures that have been damaged or have insufficient strength. Although extensive experimental investigations on the structural behavior of RC beams that are strengthened by such a method have shown that significant improvement in structural performance can be achieved under both service and ultimate conditions (Arduini, *et al*. 1997, Täljsten 1997), premature failure may occur before the ultimate flexural capacity of the strengthened RC beam is reached (Swamy, *et al*. 1987, Aprile, *et al*. 2001).

† E-mail: parkjy@skku.edu
‡ Corresponding Author, E-mail: leekm79@skku.edu
‡† E-mail: hmshin@skku.edu
‡‡E-mail: yoonje@hitel.net

(a) Shear failure

(b) Concrete cover separation

(c) Plate-end interfacial debonding

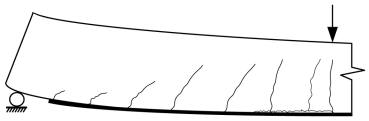

(d) Intermediate flexural crack-induced interfacial debonding

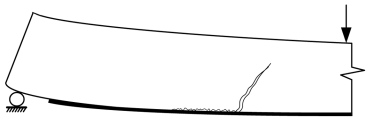

(e) Intermediate flexural shear crack-induced interfacial debonding

Fig. 1 Premature failure patterns in strengthened RC beams

A number of failure modes for RC beams that are bonded with steel or FRP soffit plates have been observed in numerous experimental studies (Ziraba, *et al.* 1995, Garden, *et al.* 1998, Nguyen, *et al.* 2001). A schematic representation of typical premature failure modes that are observed in tests is shown in Fig. 1. The premature failure modes are classifed into five main categories in the figure and they are termed (Smith and Teng 2002a, 2003b): (a) shear failure at the end of the plates, (b) concrete cover separation, (c) plate-end interfacial debonding, (d) intermediate flexural crack-induced interfacial debonding, and (e) intermediate flexural shear crack-induced interfacial debonding. Collectively, failure modes (b) and (c) are referred to as plate-end debonding failures, while failure modes (d) and (e) are referred to as intermediate crack-induced interfacial debonding failures. The debonding of the plate and the conctete causes all of the failure modes except for the shear failure mode.

All of the prematrue failure modes that are identified occur in a brittle manner, with the exception of intermediate crack-induced interfacial debonding with a long process of debonding propagation, occurs in an brittle manner. In particular, debonding at the plate ends occurs with little or no given indication of failure. Whether a particular mode is critical for a given beam depends on many parameters such as the amount of internal flexural and shear reinforcement, the geometric and material properties of the plate, the adhesive layer and the RC beam.

These premature failures must be taken into consideration for the strengthening design because they may cause brittle failure in the strengthened members before the ultimate or yield strength is reached.

Debonding failure may be caused by high bonding stresses, which are acting both parallel to the interface (shear stress) and normal to the interface (mornal stress), at the end or center of the strengthened plate. Several analytical solutions and numerical schemes have been proposed for calculating the stresses that develop at the plate-concrete interface in an uncracked RC beam (Täljsten 1997, Malek 1998).

Interfacial stress-based debonding strength models generally use interfacial stresses and bonding failure criterion for their analyses. Using the Mohr-Coulomb failure criterion, Ziraba, *et al*. (1994, 1995) and Varastehpour and Hamelin (1997) proposed the plate-end interfacial debonding model. Saadatmanesh and Malek (1998) and Tumialan, *et al*. (1999) also utilized the maximum principal stress criterion with using shear and normal stresses. Arduini, *et al*. (1997) adopted the Mohr-Coulomb failure criterion and Aprilie, *et al*. (2001) adopted the constant shear stress criterion.

We present experimental and numerical results for RC beams that are strengthened by steel or FRP plates with assuming that plate-end interfacial debonding occurs only in the direction of the shear stress along the interface. We adopted the Coulomb criterion as the failure criterion for the concrete-epoxy interface.

Diagonal shear bonding tests and flexural tests were performed to determine the primary variables for the Coulumb model, i.e., bonding properties such as the angle of internal friction and the coefficient of cohesion. Furthermore, a nonlinear finite element program, which uses an interface element with the Coulomb criterion, was developed to simulate debonding failure.

2. Analytical modeling

2.1. Debonding model

We used the interfacial stress based model as a plate debonding model with assuming that the debonding at the concrete-epoxy interface occurs parallel to the interface direction. As shown in Fig. 2, the Coulomb failure criterion with a fixed direction of failure was utilized as the bonding failure criterion. The Coulomb criterion is as follows:

$$\tau + \sigma \tan \Phi = C \tag{1}$$

where τ and σ are the peak interfacial shear and normal stresses at the concrete-epoxy interface, respectively, and Φ and C are the angle of internal friction and the coefficient of cohesion, respectively.

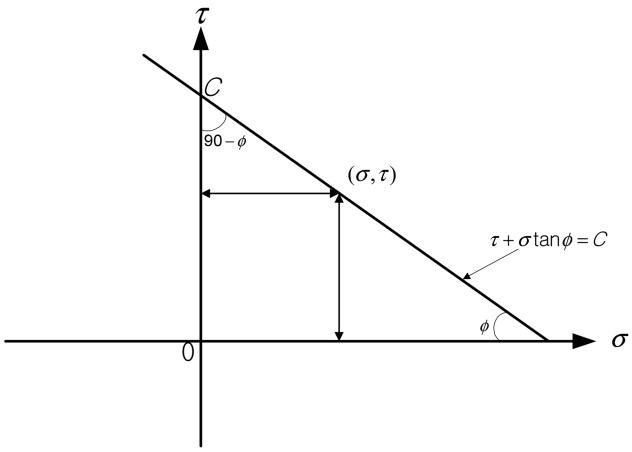

Fig. 2 Schematic representation of the Coulomb criterion

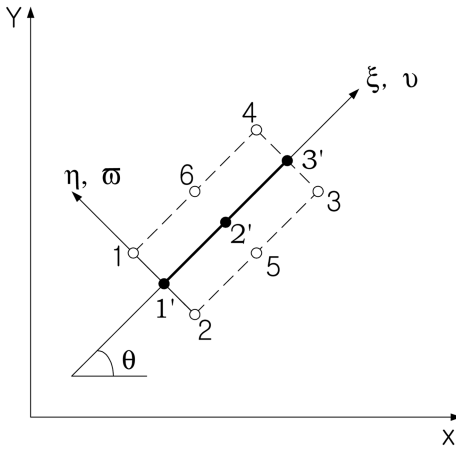

Fig. 3 Six-node interface element

2.2. Interface element formulation and material models

To formulate the normal and shear stresses that occur at the concrete-epoxy interface, a stiffness matrix for the interface element is defined as follows:

$$\begin{Bmatrix} \sigma \\ \tau \end{Bmatrix} = \begin{bmatrix} K_n & 0 \\ 0 & K_s \end{bmatrix} \begin{Bmatrix} O \\ S \end{Bmatrix} \tag{2}$$

where, K_n : E_{epoxy}/t_{epoxy}
K_s : G_{epoxy}/t_{epoxy}
E_{epoxy} : elastic modulus of the epoxy
G_{epoxy} : shear elastic modulus of the epoxy
t_{epoxy} : thickness of the epoxy layer
O : vertical displacement of the interface
S : slip of the interface

With using six node interface elements as shown in Fig. 3, it became possible to analytically calculate the shear stress that acts parallel to the interface direction together with the normal stresses, such as the peeling stress or compression stress.

The Coulomb criterion that is given in Eq. (1) is used as the material model for the interface element to simulate the debonding behavior at the concrete-epoxy interface. It is assumed that the interface element begins to yield when the shear and normal stresses at the interface, which are found from the nonlinear finite element analysis, satisfy Eq. (4). The separation of bonded steel or FRP plates can be simulated with using the yielding of these interface elements. It is also assumed that the material model of the interface element displays the characteristics that are shown in Fig. 4, where the stress increases linearly up to the maximum shear stress Eq. (3), but then it falls off exponentially beyond that point Eq. (4) The shear stress is expressed as a function of the normal stress, coefficient of cohesion and internal friction angle Eq. (5).

$$\sigma = K_n \times O,\ \tau = K_S \times S \qquad \text{for} \qquad \tau + \sigma \tan \Phi \leq C \tag{3}$$

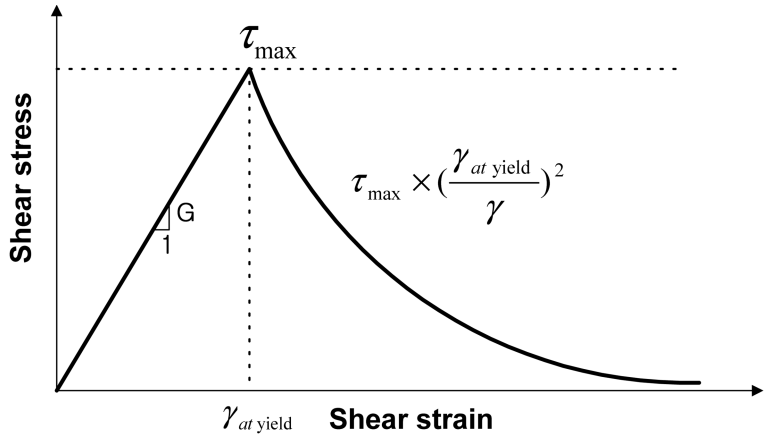

Fig. 4 Constitutive model for interface element

$$\sigma = \sigma_{max} \times \left(\frac{O_y}{O}\right)^2, \quad \tau = \tau_{max} \times \left(\frac{S_y}{S}\right)^2 \quad \text{for} \quad \tau + \sigma \tan \Phi > C \tag{4}$$

$$\tau = f(\sigma, C, \Phi) \tag{5}$$

where, σ_{max} : normal stress at $\tau + \sigma \tan \Phi = C$
τ_{max} : shear stress at $\tau + \sigma \tan \Phi = C$
O_y : vertical opening at σ_{max}
S_y : slip at τ_{max}.

2.3. Material models for concrete and reinforcing bars

The nonlinear material model for the reinforced concrete is composed of two models: (a) a model

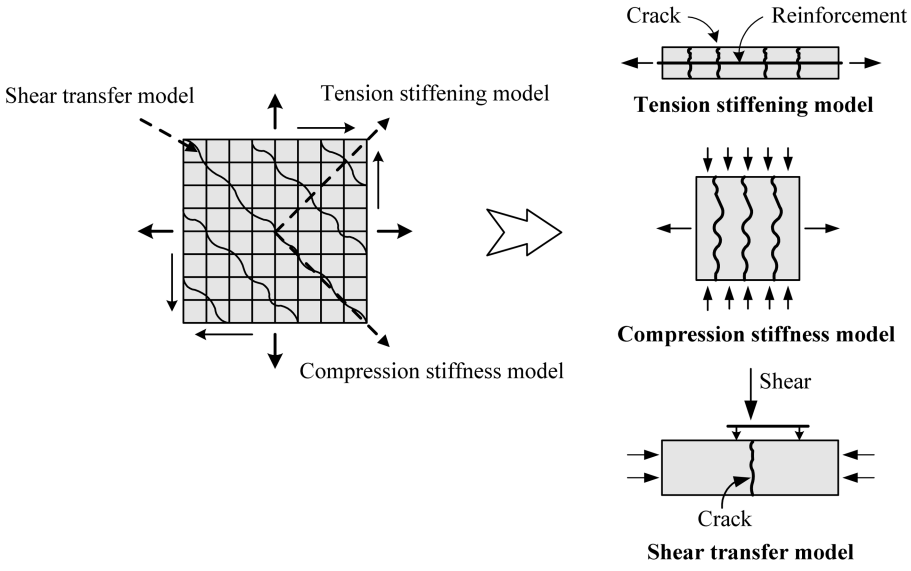

Fig. 5 Construction of cracked concrete model

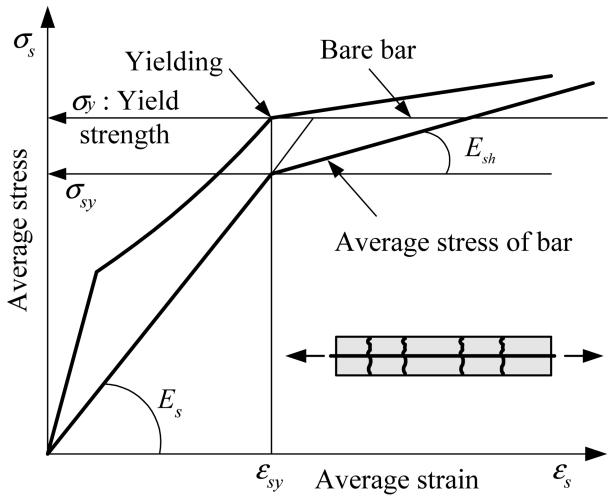

Fig. 6 Model for the reinforcing bar in the concrete

to characterize the concrete behavior; and (b) a model to characterize the reinforcing bars. For uncracked concrete, the nonlinearity and anisotropy of concrete are expressed independently of the loading history, including the strain-softening effects. A modified elasto-plastic fracture model is used to describe the behavior of concrete in the direction of the crack plane (Kim, *et al.* 2002a). The model describes the degradation in compressive stiffness by modifying the fracture parameter in terms of the strain that is perpendicular to the crack plane. The constitutive relations for reinforced concrete may be expressed through the average stress and strain based on the smeared crack concept that regards the tributary area with multiple cracks and reinforcement as a finite continuum element. The shear transfer model that is based on the contact surface density function, which is shown in Fig. 5, is used to consider the effect of shear stress transfer due to the aggregate interlock at the crack surface (Kim, *et al.* 2002b).

The stress acting on the reinforcing bar that is embedded in the concrete is not uniform, and the value is at its maximum at locations where the bar is exposed to a crack plane. The elastic relationship between the average stress and strain of thereinforcing bar is not valid when the bar yields at the crack plane, even if other sections do not yield. The post-yield constitutive law for the reinforcing bar in concrete considers the bond characteristics, as shown in Fig. 6.

2.4. Nonlinear finite element analysis program RCAHEST

RCAHEST is a nonlinear finite element analysis program for analyzing reinforced concrete structures. The proposed structural element library RCAHEST is built around the finite element analysis program shell named FEAP, developed by Taylor (2000). FEAP is characterized by modular architecture and by the facility that is used to introduce the type of custom elements, input utilities, and custom strategies and procedures.

The interface element presented above was implemented in a nonlinear finite element program based on RCAHEST that includes a plane stress element and an elasto-plastic plane stress element (Fig. 7).

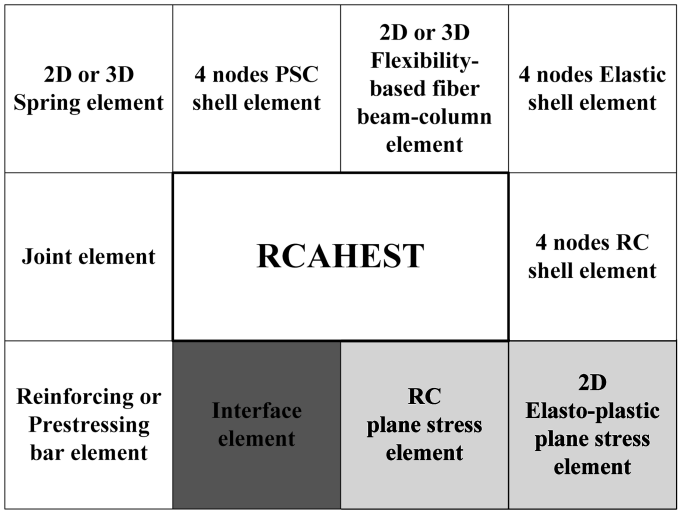

Fig. 7 Element library of RCAHEST

3. Diagonal shear bonding test

A diagonal shear bonding test was performed to determine the two bonding properties that are associated with the Coulomb criterion, the coefficient of cohesion and the angle of internal friction. The loading configuration and geometry of the specimens are shown in Fig. 6. Prismatic concrete elements were cast with different inclination angles of α = 30°, 45° and 60° for both the shear-compression and shear-tension tests. Two elements with the same inclination angle were attached together with a 3-mm thick layer of the epoxy that was used for bonding the plates. As shown in Fig. 8, steel bars were embedded in the top and bottom sides of the specimens for the uniaxial tensile test. Table 1 shows the material properties of the concrete and epoxies.

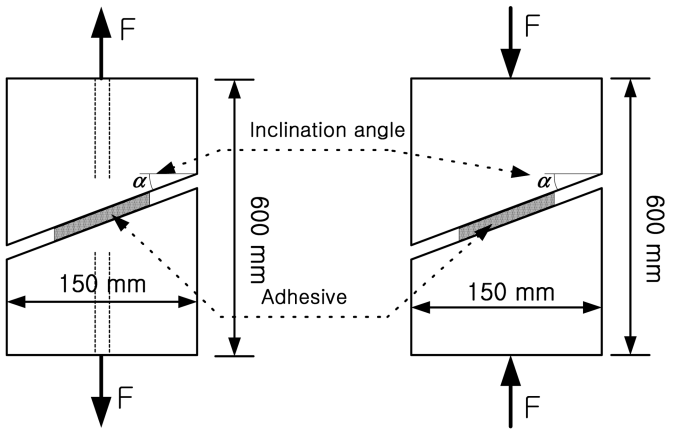

(a) Tension + shear (b) Compression + shear

Fig. 8 Loading configuration and geometry of the diagonal shear specimens

Table 1 Properties of concrete and adhesives

Material	Compressive strength (MPa)	Tensile strength (MPa)	Modulus of elasticity (GPa)	Bonding strength (MPa)
Concrete	52.3	3.7	30.6	-
Grout	-	41.5	1.3	> 8.3

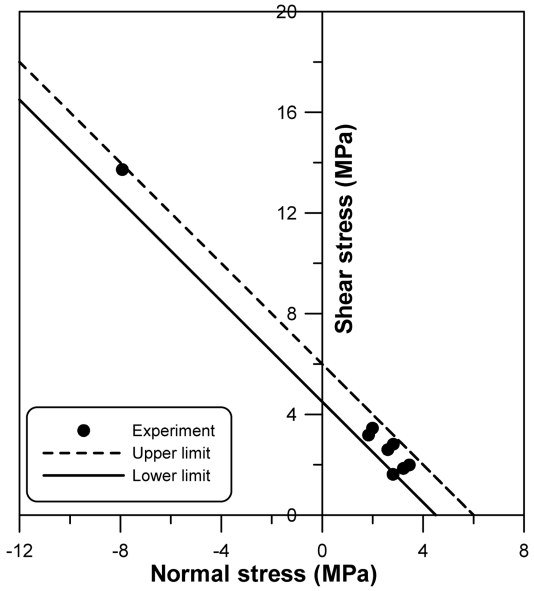

Fig. 9 Coulomb failure envelope for the epoxy-concrete interface

Fig. 9 shows the normal strengths, which are the tensile and compressive strength, defined as $\sigma = F \times \cos \alpha / A$ and the shear strength, defined as $\tau = F \times \sin \alpha / A$, for eight specimens. The Coulomb failure envelope for the concrete-epoxy interface was constructed by using a regression analysis with 96% probability with assuming that the probability distibution for the experimental results was a nomal distribution. A shear-tension test was performed because most debonding failures occurs in the tensile zone of RC beams. From the envelope, it can be deduced that the angle of the internal friction and the range of the coefficient of cohesion are set to 45° and 4.5~6.0 MPa, respectively.

4. Flexural test of beams strengthened by externally bonded steel plates

A flexural test was carried to investigate the premature failure behavior of RC beams strengthened by externally bonded steel plates that are 2,200 mm long RC beam with a rectangular 150 mm by 250 mm cross section. The material properties of the concrete and epoxies that were used for the test beams were the same as those that were used in the diagonal shear bonding test. Two 13 mm diameter bars (A_s = 254.3 mm^2) and two 10 mm diameter bars (A_s = 143 mm^2) were used as the tensile and compression steel bars, respectively. In order to prevent the shear failure of the beam, 10

Table 2 Details of Series I, II and Series III beams

Series	Beam type	Plates length (mm)	Plate thickness (mm)	Epoxy thickness (mm)	Beam length (mm)	Comp. strength of con. (MPa)*	Yield strength of bar (MPa)	Yield strength of plate (MPa)
I (Present study)	Control	-	-	-	2,000	52.3	343	-
	S3-150	1,500	3.0	3.0	2,000	52.3	343	265
	S3-190	1,900	3.0	3.0	2,000	52.3	343	265
	S6-190	1,900	6.0	3.0	2,000	52.3	343	265
II (Swamy, *et al.* 1987)	201	2,200	-	-	2,300	63.9	470	-
	203	2,200	1.5	1.5	2,300	63.3	470	236
	204	2,200	3.0	1.5	2,300	66.4	470	258
	205	2,200	6.0	1.5	2,300	70.2	470	248
	207	2,200	1.5	3.0	2,300	70.2	470	236
	208	2,200	3.0	3.0	2,300	68.0	470	258
	209	2,200	6.0	3.0	2,300	72.2	470	248
	216	2,200	1.5	6.0	2,300	68.4	470	236
	217	2,200	3.0	6.0	2,300	68.6	470	258
	218	2,200	6.0	6.0	2,300	71.5	470	248
III (Park, *et al.* 2002)	Cont213	-	-	-	3,400	26.7	467.7	-
	Cplp213	2,900	3.0	3.0	3,400	26.7	467.7	2803
	Cont221	-	-	-	3,400	35.0	467.7	-
	Cplp221	2,900	6.0	3.0	3,400	35.0	467.7	2803
	Con227	-	-	-	3,400	40.4	467.7	-
	Cplp227	2,900	1.5	3.0	3,400	40.4	467.7	2803

*Cylinder compressive strength for series I and III, and Cubic compressive strength for series II.
**Steel plate used for series I and II, and FRP plate used for sereis III.

mm diameter stirrups were placed with the spacing of 100 mm. Four point loading was applied with a 200 mm spacing from the center of a beam.

Table 2 shows the epoxy layer thickness, the plate length, and the plate thickness for the four beam types. A strengthened beam with the plate length of 1,500 mm and the epoxy layer thickness of 3 mm was designated as S3-150. The steel plates width of all beamms is 130 mm. Other beam types were designated as S3-150 and S6-190 corresponding to the the plate length and the epoxy layer. Load versus deflection curves for the tested beams were monitored using a load cell and three LVDT's that were installed in the center zone of the beam. The failure behavior of the strengthened beams was also observed and the strains of the steel plate were measured by attaching the strain gauges with a spacing of 50 mm. The shear stress at the interface was obtained from the measured strains of the strengthened steel plate as follows:

$$\tau_{epoxy} = \frac{\Delta\varepsilon E_{sp} t_{sp}}{\Delta L} \tag{5}$$

where, τ_{epoxy} : shear stress of the epoxy
$\Delta\varepsilon$: strain difference between two adjacent gauges

Table 3 Experimental loads and deflections of Series I beams

Beam type	Plate thickness (mm)	At first crack		At yielding of steel bar and (steel plate)		At maximum load	
		Load (kN)	Deflection (mm)	Load (kN)	Deflection (mm)	Load (kN)	Deflection (mm)
Control	-	15.5	0.8	37.4 (–)	4.5 (–)	54	26.0
S3-150	3	25.2	0.8	– (82.9)	– (4.5)	91	5.2
S3-190	3	24.5	0.8	91.2 (80.0)	4.3 (3.8)	120	17.0
S6-190	6	44.7	1.0	– (120.7)	– (4.7)	130	5.1

ΔL : distance between two adjacent gauges
E_{sp} : elastic modulus of the steel plate
t_{sp} : thickness of the steel plate.

Table 3 shows the load and deflection at the first cracking, yielding, and the failure of the tested beams. A control beam that was not strengthened showed ductile failure behavior as we had expected. Beam S3-150 showed bonding failure after the yielding of the externally bonded steel

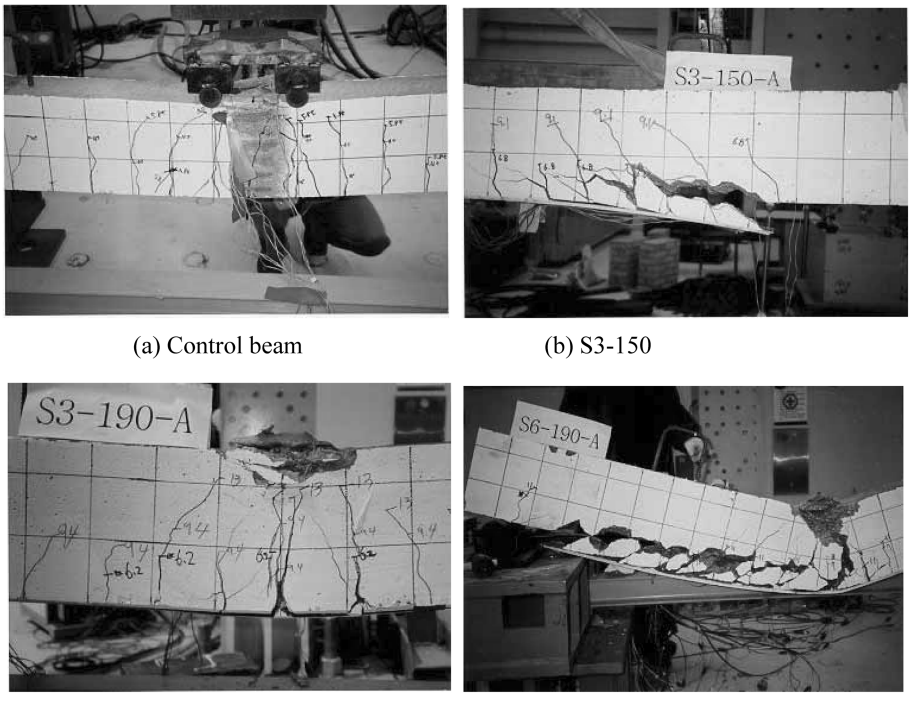

(a) Control beam (b) S3-150

(c) S3-190 (d) S6-190

Fig. 10 Crack patterns and failure modes for the Series I beams

plate, while beam S3-190 showed a typical ductile failure behavior after both the steel plate and tension steel yielded. The loading capacity of beam S3-150 increased 69% compared with that of the control beam. The loading capacity of beam S3-190 was 32% higher compared to that of beam S3-150, which implies that the bonding length is an important factor for the strengthening design. The debonding of beam S6-190 occurred the steel plate yielded, but before the tensile steel yielding.

The crack and failure patterns of the beams are shown in Fig. 10; note the typical brittle failure pattern of Fig. 10(b) and Fig. 10(d).

5. Nonlinear analysis of RC beams strengthened by externally bonded plates

5.1. Detail and geometry of RC beams for FEM modeling

Four beams of Series I that were tested in the present study, ten beams of Series II that were tested by Swamy, *et al*. (1987) and six beams of Series III that were tested by Park, *et al*. (2002) were numerically anlayzed to obtain the bonding properties of the concrete-epoxy interface. All of the beams in Series II were reinforced with three 20 mm diameter bars at an effective depth of 220 mm. The shear spans were provided with 6 mm diameter stirrups at 75 mm center to center. The epoxy resin that was used in the Series II beams had a tensile strength of approximately 15.0 MPa and an elastic modulus of 2.1 GPa. All of the beams in Series III were reinforced with three D10 bars at an effective depth of 270 mm. The shear spans were provided with D10 stirrups at 100 mm center to center. The epoxy resin that was used in the Series III beams had a tensile strength of approximately 24.8 MPa and an elastic modulus of 45.05 GPa.

For modeling the beams used in the experiment, plane stress elements with nonlinear material models were used for the concrete, steel bar, and steel or FRP plate, and the interface elements that were presented in this paper were used for the concrete-epoxy interface. For the finite element mesh generation of each beam, 176~266 nodes and 147~194 elements were used.

5.2. Comparison of analytical and experimental results

Fig. 11 shows the load-deflection curves that were obtained from the finite element analysis for the four Series I beams. For the control beam and beam S3-190, which showed flexure failure, the analysis results matched well with the experimental results.

Fig. 12 shows the shear stress distribution along the concrete-epoxy interface for beam S3-150 and beam S3-190. Figs. 12(a) and 12(b) compare the experimental results with the FEM analysis results for beam S3-150 and beam S6-190. The shear stress is at its maximum at a location that is close to the end of the steel plate and it decreases towards the center of the beam.

In order to numerically determine the shear stress distribution along the interface, finite element analysis of beams that were strengthened by externally bonded steel plates was carried out with using the displacement incremental method and newton method for the convergence of the solution. For beam S3-150, the first cracking at the concrete-epoxy interface occurred at a load of 86.4 kN and debonding gradually moved inside the beam (Fig. 12a). At a maximum load of 92.4 kN, the debonding moved rapidly and the load decreased. For S6-190, the first cracking at the the concrete-epoxy interface occurred at the maximum load and the debonding failure occurred abruptly (Fig. 12b).

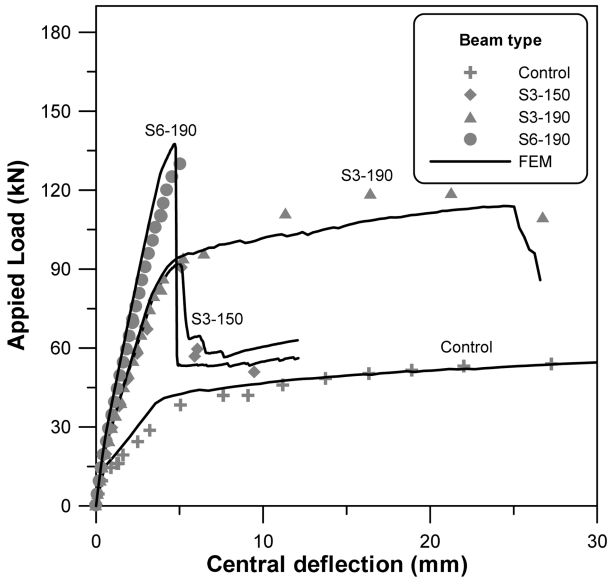

Fig. 11 Load-deflection curves for the Series I beams

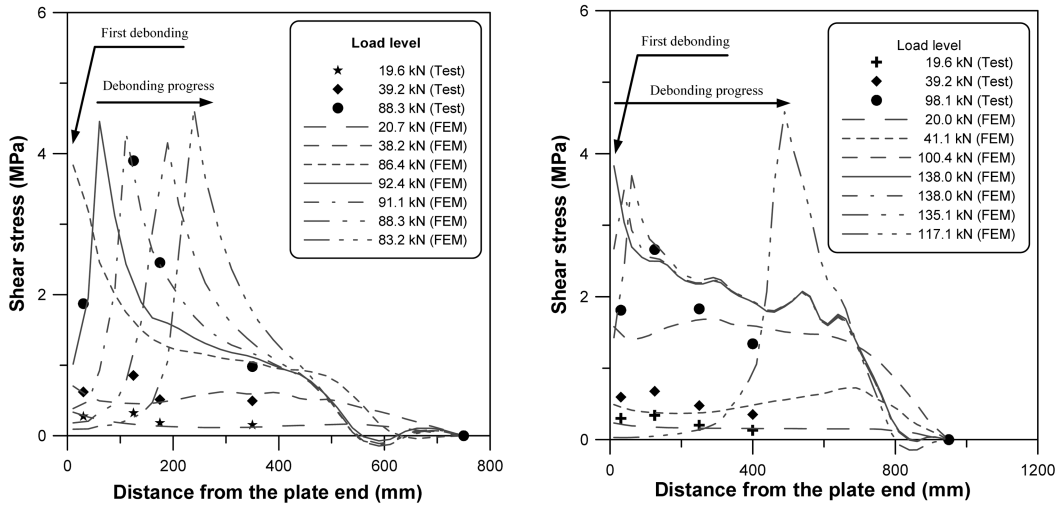

(a) S3-150 (b) S6-190

Fig. 12 Shear stress distribution along the concrete-epoxy interface

With comparing the debonding behavior between beam S3-150 and beam S6-190, the difference is due to the shear stress distribution as the shear stress gradient for beam S3-150 is greater than it is for beam S6-190, which results from the difference of the length and thickness of the plate. Consequently, the loading capacity after the first debonding occurs is greater for beam S6-190 than it is for beam S3-150.

Fig. 13 shows the analytical and experimental load-deflection curves for the four Series II beams(beam 201, 203, 204, and 205). For the control beam (201) and beam 203, which showed

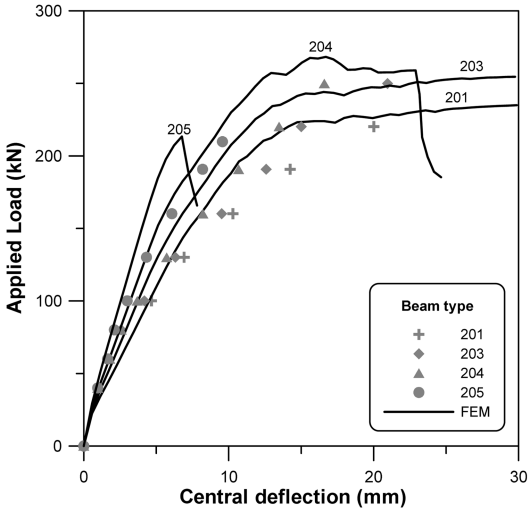

Fig. 13 Load-deflection curves for the Series II beams

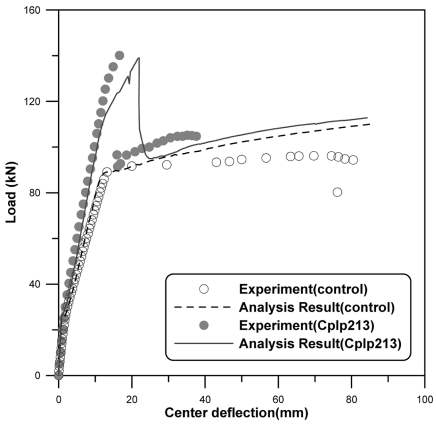

(a) Cplp213

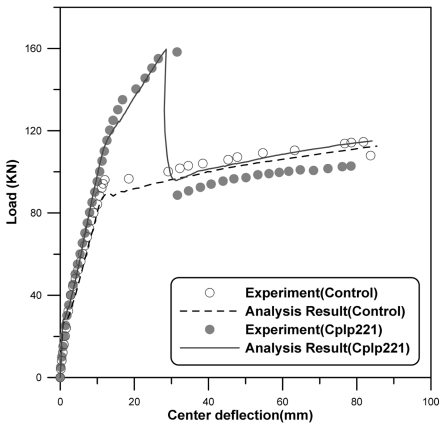

(b) Cplp221

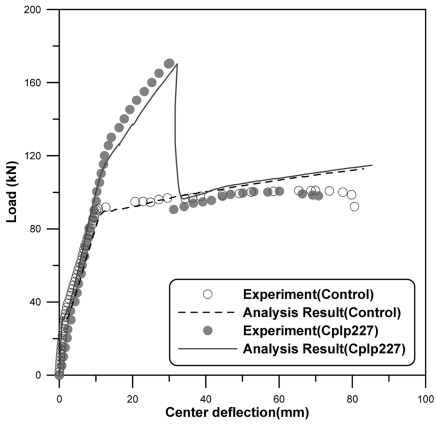

(c) Cplp227

Fig. 14 P-D curves for the Series III beams

flexural failure, although the analytical load-deflection curves agreed well with the experimental results from the initial stiffness and yielding behavior up to the ultimate load, the tangential slopes after cracking were stiffer for the analytical results than they were for the experimental results.

Fig. 14 shows the result of the Series III beams (Cplp213, Cplp221 and Cplp227) which are the FRP plates that are used for strengthening the RC beams.

5.3. Premature loads and debonding properties

Premature failure due to debonding is effectively predicted for beams S3-150 and S6-190, where the coefficients of cohesion were set to 5.0 MPa and 4.7 MPa, respectively. For beam S3-190, the shear and normal stresses are 2.69 MPa and 0.21 MPa at the plate-end, respectively; that is, the coefficient of cohesion for the concrete-epoxy interface of beam S3-190 should be greater than 2.9 MPa.

For the case of beam 204, analytical and experimental results showed bonding failure following flexural failure when the coefficient of cohesion was set to 5.5 MPa. For the beam 205, the analytical result matched well with the premature load when the coefficient of cohesion was also set to 5.5 MPa.

For the case of beams Cplp213, Cplp221 and Cplp227, both the analytical and experimental results showed bonding failure following flexural failure when the coefficient of cohesion was set to 5.0 MPa, 5.3MPa and 5.2 MPa, which matched well with the premature load.

Table 4 Comparison between flexure failure specimens and finite element analysis

Series	Beam type	Experiment ultimate load (1) (kN)	Analysis ultimate load (2) (kN)	Max. stress at interface		Coef. of cohesion (MPa)	Failure mode	(1)/(2)
				Shear stress (MPa)	Normal stress (MPa)			
I	Control	54	55	-	-	-	Flexure	0.98
	S3-190	120	114	2.7	0.2	4.5	Flexure	1.05
	S3-150	91	92	4.5	0.5	5.0	Debond	0.99
	S6-190	130	138	4.0	0.7	4.7	Debond	1.05
II	201	232	235	-	-	-	Flexure	0.99
	203	270	255	3.9	0.2	4.5	Flexure	1.06
	204	270	268	5.2	0.3	5.5	Debond	1.01
	205	213	213	5.0	0.5	5.5	Debond	1
	207	262	258	3.2	0.1	-	Flexure	1.02
	208	264	265	5.0	0.4	5.4	Debond	1.04
	209	220	219	5.0	0.6	5.6	Debond	1.00
	216	262	288	2.6	0.1	4.5	Flexure	0.91
	217	257	261	4.4	0.2	4.6	Debond	1.02
	218	194	204	4.1	0.4	4.5	Debond	1.05
III	Cplp213	140	138	4.7	0.2	5.0	Debond	1.01
	Cplp221	158	160	5.2	0.1	5.3	Debond	1.06
	Cplp227	171	170	5.1	0.1	5.2	Debond	0.99

Table 4 lists the ultimate loads that were obtained from the experimental and finite element analysis, the maximum stresses at the concrete-plate interfaces, the coefficient of cohesion, and the failure modes for the test Series I, II and III beams. Note that the analytical results closely follow the experimental data for the eight beams that showed premature failure.

For the beams that had premature failure due to debonding, the corresponding coefficient of cohesion value was found to be between 4.5 and 5.6 MPa when the angle of internal friction was set to 45°. These numbers fall within the range found from the diagonal shear test. Taking into account many variables, such as the thickness and the bonding length of the plate, the coefficient of cohesion for beams with externally bonded plates ranges between 4.5 and 6.0 MPa.

6. Conclusions

The following conclusions can be drawn;

(1) The Coulomb criterion as a debonding failure criterion was proposed and an interface element that utilized this model was implemented in a nonlinear finite element program (RCAHEST) to analytically examine the premature failure of strengthened RC beams. The analytical models that were used in the program involve the nonlinear material models for constituent materials and the characteristics of the concrete-epoxy interface.

(2) Flexural test on RC beams showed that the ultimate load and the postcracking stiffness of strengthened RC beams increases considerably compared with control RC beams. The epoxy-concrete interface behavoir of RC beams strengthened by externally bonded plates was simumated by analysis results obtained from the nonlinear finite element analysis program with the proposed models.

(3) Experiment and analysis work lead to the corresponding range for the coeffient of cohesion value (4.5~6.0 MPa) for beams strengthened by externally bonded plates. A reliable strengthening design can be achieved by predicting the premature failure loads of strengthended RC beams using the bonding properties and the finite element program.

Acknowledgements

The study described in this paper was supported by the Ministry of Construction and Transportation through the Korea Bridge Design and Engineering Research Center. The authors wish to express their gratitude for the support received.

References

Aprile, A., Spancone , E. and Limkatanyu, S. (2001), "Role of bond in RC beams strengthened with steel and FRP plates", *J. Struct. Eng.*, ASCE, **127**(12), 1445-1452.

Arduini, M., Tommaso, A. D. and Nanni, A. (1997), "Brittle failure in FRP plate and sheet bonded beams", *ACI Struct. J.*, **94**(4), 363-370.

Garden, H. N., Quantrill, R. J., Hollaway, L. C., Thorne, A. M. and Parke, G. A. R. (1998), "An experimental study of the anchorage length of carbon fibre composite plates used to strengthen reinforced concrete beams", *Const. Build. Mater.*, **12**, 203-219.

Kim, T. H., Lee, K. M., Yoon, C. Y. and Shin, H. M. (2002a), "Inelastic behavior and ductility capacity of reinforced concrete bridge piers under earthquake. I: Theory and Formulation", *J. Struct. Eng.*, ASCE, **129**(9), 1199-1207.

Kim, T. H., Lee, K. M. and Shin, H. M. (2002b), "Nonlinear analysis of reinforced concrete shells using layered elements with drilling degree of freedom", *ACI Struct. J.*, **99**(4), 418-426.

Nguyen, D. M., Chan, T. K. and Cheong, H. K. (2001), "Brittle failure and bond development length of CFRP-concrete beams", *J. Compos. Constr.*, ASCE, **5**(1), 12-17.

Malek, A. M., Saadatmanesh, H., and Ehsani, M. R. (1998), "Prediction of failure load of R/C beams strengthened with FRP plate due to stress concentration at the plate end", *ACI Struct. J.*, **95**(1), 142-152.

Park, Y. H., Kim, K. H., Yoo, Y. C., Park, J. S., Cho, C. J. and Chung, W. T. (2002), *Development of Strengthening Methods for Deteriorated Concrete Bridges*, Korea Institute of Construction Technology 2002-051, Internal Research Project Report.

Roberts, T. M. (1989), "Approximate analysis of shear and normal stress concentrations in the adhesive layer of plated RC beams", *The Struct. Eng.*, **67**(12), 229-233.

Saadatmanesh, H. and Malek, A. M. (1998), "Design guidelines for flexural strengthening of RC beams with FRP plates", *J. Compos. Constr.*, ASCE, **2**(4), 158-164.

Smith, S. T. and Teng, J. G. (2002), "FRP strengthedned RC beams-I: review of debonding strength models", *Eng. Struct.*, **24**(4), 385-395.

Smith, S. T. and Teng, J. G. (2002), "FRP strengthened RC beams-II: assessment of debonding strength models", *Eng. Struct.*, **24**(4), 397-417.

Swamy, R. N., Jones, R. and Bloxham, J. W. (1987), "Structural behaviour of reinforced concrete beams strengthened by epoxy-bonded steel plates", *The Struct. Eng.*, **65A**(2), 59-68.

Taylor, R. L. (2000), *FEAP - A Finite Element Analysis Program, Version 7.2,* Users Manual, Volume 1 and Volume 2.

Täljsten, B. (1997), "Strengthening of beams by plate bonding", *J. Mater. Civ. Eng.*, ASCE, **9**(4), 206-212.

Tumialan, G., Belarbi, A. and Nanni, A. (1999), *Reinforced Concrete Beams Strengthened with CFRP Composites: Failure Due to Concrete Cover Delamination*, Department of Civil Engineering, Center for Infrastructure Engineering Studies, Report No. CIES99/01, University of Missouri-Rolla, USA.

Varastehpour, H. and Hamelin, P. (1997), "Strengthening of concrete beams using fiber-reinforced plastics", *Mater. Struct.*, **30**, 160-166.

Ziraba, Y. N., Baluch, M. H., Basunbul, I. A., Sharif, A. M., Azad, A. K. and Alsulaimani, G. J. (1994), "Guidelines towards the design of reinforced concrete beams with external plates", *ACI Struct. J.*, 91(6), 639-646.

Ziraba, Y. N., Baluch, M. H., Basunbul, I. A., Azad, A. K., Al-Sulaimani, G. J. and Sharif, A. M. (1995), "Combined experimental-numerical approach to characterization of steel-concrete interface", *Mater. Struct.*, **28**, 518-525.

CC